Multi-Resistant Radar Jamming Using Genetic Algorithms

Hans J. F. Moen
Norwegian Defence Research Establishment
P.O.Box 25, NO-2027 Kjeller, Norway
jonas.moen@ffi.no

Stein Kristoffersen
Norwegian Defence Research Establishment
P.O.Box 25, NO-2027 Kjeller, Norway
stein.kristoffersen@ffi.no

ABSTRACT
The next generation of advanced self-protection jammers is expected to deliver effective and energy efficient jamming against modern air tracking radars. However, optimizing such experimental jammers is a challenging task. In this paper the novelty and applicability of using genetic algorithms (GA) for developing advanced digital radio frequency memory jammer techniques against radars employing the constant false alarm rate detection algorithm are demonstrated. It is shown how GA can handle the large and complex solution space of the problem, finding a Pareto front in the problem domain of jammer transmitting power versus detectability, producing new jamming techniques and fresh insight into the complex radar-jammer dynamics. As a main result, it is demonstrated how GA is capable of producing effective multi-resistant jamming techniques. This is an important jamming property when operating against uncertain radar detection algorithms in real world scenarios. Furthermore, single- and multi-resistant jamming techniques are shown to handle noisy environments, and the important issue of jamming robustness against varying target radar cross section is addressed. The energy efficiency of GA jamming techniques is investigated by comparing the efficiency of more conventional noise jamming techniques.

Categories and Subject Descriptors
G.1.6 [**Numerical Analysis**]: Optimization; I.2.8 [**Artificial Intelligence**]: Problem Solving, Control Methods, and Search; J.7 [**Computer Applications**]: Military

General Terms: Design, Performance

Keywords: Jamming technique design, Digital RF Memory, pulse-Doppler radar, constant false alarm rate, genetic algorithm, multi-objective optimization, multi-resistant optimization

1. INTRODUCTION
Advanced digital radio frequency memory (DRFM) self-protection jammers [4, 7, 10] against radars promise much lower energy output compared to conventional noise jammers [5] and are capable of producing far more complex jamming signals than standard DRFM jammers [11]. The radar-jammer dynamics of such a self-protection system are illustrated in Figure 1. In this setting the radar transmits a waveform and receives echoes from the target and a self-protection jammer on-board the target. In addition there are clutter reflections and thermal noise in the system, forcing some kind of noise filtering on the radar echo signal for target detection and tracking. One of the most commonly employed automatic detection methods is the constant false alarm rate (CFAR) detection algorithm [12]. The purpose of the on-board jammer is to manipulate the received radar signal in order to deny the radar detecting and tracking the target. The complexity of the problem makes it difficult to use conventional optimization methods for technique development as it is hard to obtain mathematical descriptions of the system as a whole. In addition, the solution space is vast, could be non-linear and may contain a multitude of local optima. This results in the need for alternative methods for realizing the full potential of this type of jammers.

Genetic algorithms (GA) [2] offer efficient and robust global optimization inspired by the theory of evolution. Previous studies [3, 6, 9] demonstrate the feasibility of using GA in developing electronic countermeasures (ECM) techniques for range-gate pull-off against tracking radars using standard DRFM jammers. The aim of this study, however, is to demonstrate the applicability of using GA for developing promising counter detection jamming techniques for the next generation of advanced DRFM jammers.

We look primarily for new types or 'structures' of jamming techniques and are not that concerned about convergence speed, finding optimal parameters or performing complete analysis of all results.

In this paper the MATLAB Genetic Algorithm Toolbox [8] has been used for all simulations.

Section 2 explains the radar and jammer modeling and section 3 introduces the important jammer objective list stating what we want to achieve. In section 4 the case of single-resistant jamming is investigated, i.e. radar CFAR algorithm is known, before multi-

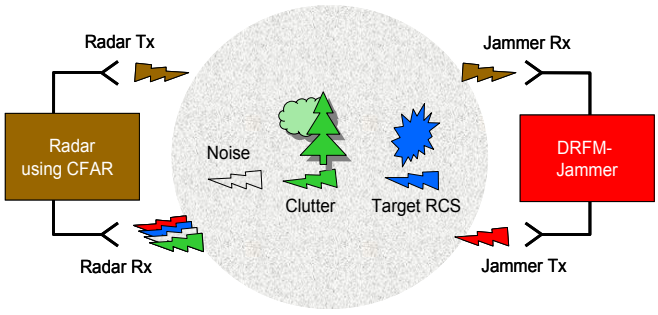

Figure 1: Radar-jammer dynamics. Radar transmits a waveform (brown) and receives echoes from target (blue), jammer (red) and clutter (green). In addition there is thermal noise in the system (grey).

GECCO'08, July 12–16, 2008, Atlanta, Georgia, USA.

resistant jamming is explored in section 5. Both cases are analysed for robustness against noise and variations in target radar cross section (RCS). Finally, findings are summarized and conclusions are drawn in section 6.

2. RADAR AND JAMMER MODELING

In this study advanced DRFM jamming for self-protection against modern coherent pulse-Doppler radars is investigated.

2.1 Constant PRI Pulse-Doppler Radar

Pulse-Doppler radars usually coherently process batches or bursts of pulses with constant pulse repetition interval (PRI), as illustrated in Figure 2a. The radar takes complex samples of the received signals at a rate consistent with one complex sample per range resolution cell. This signal vector is folded at the PRI rate to position all samples from the same range in the same column, Figure 2b. After folding, a fast Fourier transform (FFT) is applied to each range column to separate signal components with different Doppler frequency offset. A radar range-Doppler (RD) matrix of amplitudes then results from one coherent processing interval, Figure 2c.

Thermal noise in the radar RD matrix can be modeled as white noise given by [12]

$$A_{i,j} = N(0,\sigma) \quad (1)$$

where $A_{i,j}$ is amplitude for pixel i,j in radar RD matrix given by a normal noise statistics with mean 0 and standard deviation σ. The energy deposited in the radar RD matrix is the sum of all squared RD cells.

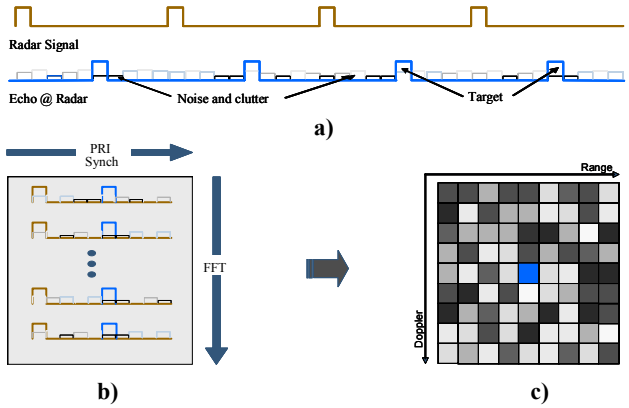

Figure 2: a) constant PRI puls-Doppler radar signal and echo b) folded at the PRI rate and a FFT is applied to the Doppler axis producing c) an amplitude radar RD matrix.

2.2 Radar CFAR Processing

Modern radars typically use CFAR processing [12] to declare detections in the radar RD matrix as illustrated in Figure 3a. CFAR calculates the ratio of the amplitude in a cell under test (CUT) relative to a local background, illustrated by the green CFAR frame in Figure 3b. There are also radars using one-dimensional CFAR, range only frame or Doppler only frame. The local background level can be calculated in a number of ways. Computing the mean amplitude in a number of neighboring RD cells is the most common. This version of CFAR is called cell averaging CFAR or CA-CFAR and is used throughout this paper. Typically there are guard gates adjacent to the CUT to avoid leakage from the CUT contributing to the local background, which might reduce sensitivity to targets straddling the resolution cells. This calculation is done for all RD cells and results in a new radar RD CFAR ratio matrix as seen in Figure 3c, which is usually thresholded to produce a CFAR detection matrix.

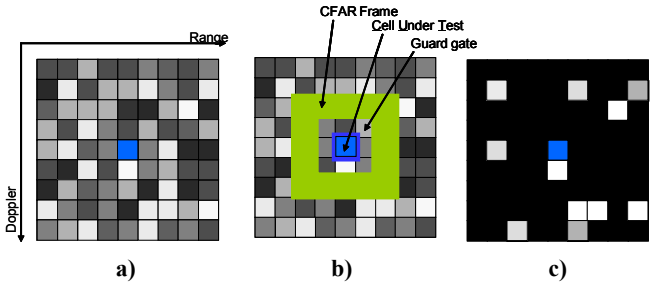

Figure 3: a) CFAR processing of a radar RD matrix b) using 5×5 CFAR frame giving c) a radar RD CFAR ratio matrix.

2.3 Advanced DRFM Jammer

An advanced DRFM based radar jammer stores a copy of each radar pulse and uses it as the basis signal for the jamming signal [11]. The stored radar signal can be delayed, amplitude modulated and its frequency can be changed. These modifications are done to produce a false target with parameters different from the real target being protected by the jammer. A fundamental limitation in standard DRFMs is that at a given time instant only one set of modulation parameters can be applied, i.e. single delay, amplitude and Doppler. The advanced DRFM jammer can produce multiple simultaneous overlapping jamming pulses with individual modulation parameters through an additional modulator. This type of DRFM jammer has been described in the context of countermeasures to imaging radars in [4, 7, 10]. The modulator is illustrated in Figure 4a with a possible radar RD matrix in Figure 4b resulting from jamming, where jammer affected RD cells are in red. The effect of the advanced DRFM jammer on a pulse-Doppler radar can be modeled by generating a separate complex RD matrix resulting from the jamming and adding it to the radar RD matrix. This assumes the jammer can produce its RD matrix synchronized with the radar matrix, with the same resolution in both directions.

The jammer matrix is coded as a chromosome of dimension $32 \times m \times n$ bits, where m is the number of range cells and n is the number of Doppler cells in the jammer signal. Each $A_{i,j}$ amplitude RD cell in the jammer matrix has fixed chromosome position when converting from genotype to phenotype.

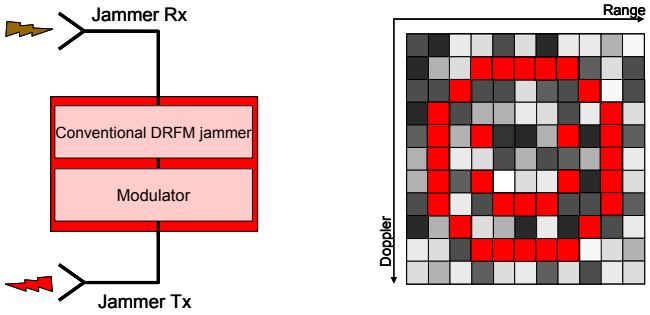

Figure 4: a) advanced DRFM jammer and b) the radar RD matrix affected by jamming in red.

3. JAMMER OBJECTIVES

The main objective of self-protection jamming is to deny radar detection of the target in a real environment without producing new detections on the jamming signal. In addition the jamming signal should not trigger warning functions in the radar. Moreover, this should be done robustly at 'minimum cost' to the jammer. Hence, the jamming should

1. suppress target detection and not produce new detections in a realistic noisy environment with dynamic target RCS using lowest possible transmitting power,
2. be robust against a broad range of radar CFAR detection algorithms, i.e. multi-resistant jamming,
3. be robust against variations in radar and jammer parameters.

4. SINGLE-RESISTANT JAMMING

In this section the first and primary objective of the jammer objective list is addressed. Known radar CFAR detection algorithm is assumed. For every generation in the GA each individual, which represents a particular jamming technique, produces a corresponding radar RD CFAR ratio matrix, forming the basis for the fitness evaluation. In this case fitness is set to R_{max}, which is the maximum value of the radar CFAR ratio matrix. MATLAB pseudo code for the simulation is shown below.

```
for i=1:populationSize %loop over population
 GetJammerRDMatrix(GetChromosome(population,i))
 GetRadarRDMatrix(JammerRDMatrix,TargetRDMatrix)
 GetRadarCFARRatioMaxtrix(RadarRDMatrix,CFARtype)
 F=max(RadarCFARRatioMaxtrix) %report fitness
end
```

The target is always in the centre of the radar RD matrix and the jamming matrix is centered on the target. The jamming matrix is smaller than the radar RD matrix leaving the outermost cells of the radar RD matrix unaffected by the jamming signal matrix. Target amplitude is 100 unless otherwise stated. In Table 1 MATLAB GA Toolbox parameter settings for single-objective simulations are presented.

Table 1: MATLAB GA Toolbox parameters

Creation:	Uniform	Interval [0,1]	Population Size 100
Selection:	Stochastic Uniform	Rank Fitness Scaling	Elite Count 2
Crossover:	Scattered	Crossover Fraction 0.8	
Mutation:	Gaussian	Scale 1	Shrink 0

4.1 The Pareto Front

As a starting point for evaluating jammer matrices a large jammer matrix of size 95×127 is used. A CFAR frame of 5×5 for radar target detection is chosen as it offers the most general CFAR algorithm with low order and 2-dimensional properties and the intuitive R_{max} is used as the fitness function.

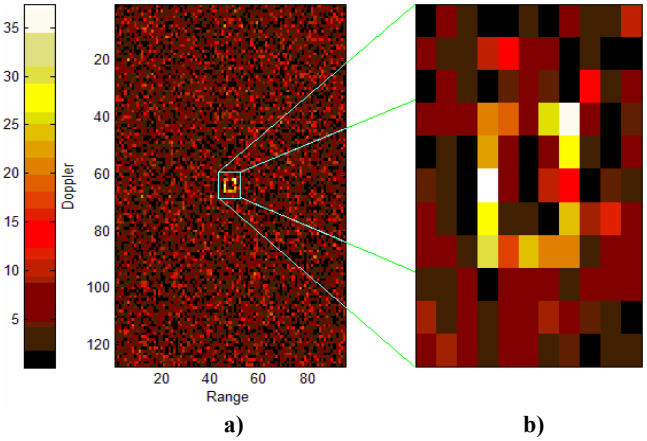

Figure 5: A jamming matrix of size 95×127 **after** 156 **generations giving** J/S=34.8804 **and** R_{max}=4.4053**. Figure a) shows the entire jammer matrix and b) shows the target-centered** 11×11 **sub-matrix.**

In Figure 5 it is shown how the GA generates a 'structure' in the jamming matrix positioned on the CFAR frame around the target and a noise-like signal elsewhere. Simulation was run for 156 generations producing a total of 0.18×10^9 CFAR ratio calculations or 0.18 CRC. This structure suppresses target detection and its fine details along with the corresponding noise-like surroundings ensure that no additional detections occur above a CFAR threshold of 4.4053. This is done at the relatively small energy expenditure for the jammer signal of J/S~35 times the target echo at the radar. Nevertheless, the jammer matrix is probably larger than necessary, producing noise-like signals or 'genetic noise' far from the central structure of the jammer signal, increasing J/S for a given detectability or R_{max}. Hence, the effect of jammer matrix size on the jammer signal needs to be studied.

Figure 6 shows J/S versus R_{max} for seven different jamming matrix sizes. The plot shows the fundamental inverse relation between jamming signal power and detectability; higher jammer power results in lower detectability and vice versa, making the problem domain that of a multi-objective optimization problem with J/S and R_{max} as objectives. Furthermore, no jamming matrix size is optimal over all values for J/S and R_{max} since none of the jammer matrix lines represents a Pareto front alone.

Small matrices are preferable when low J/S is required, while larger matrices can achieve better performance in terms of low R_{max}. This might be due to small jamming matrices having limited available state space at high energies, resulting in higher energy density for a given R_{max}. A jamming matrix size of 11×11 seems as a robust and flexible matrix size for further studies as it has good overall performance against the 5×5 CFAR frame.

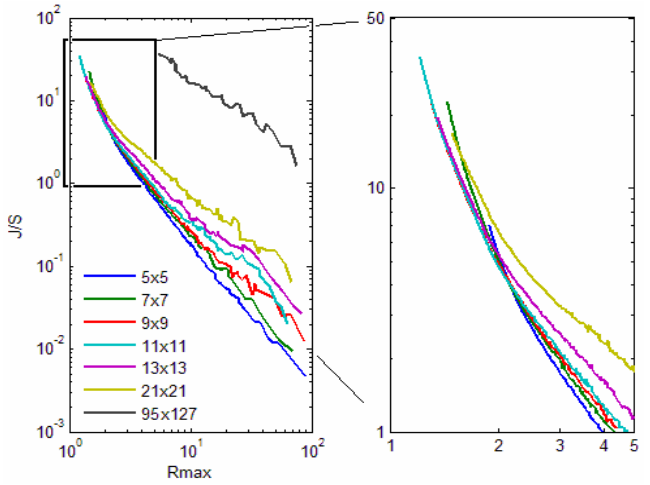

Figure 6: Jammer matrix size analysis. a) shows the entire domain of *J/S* and R_{max}, whereas b) shows the most interesting portion of the same domain. Both plots use logarithmic scales.

The different plots of Figure 6 have all been produced by 'growing' solutions, using a uniform creation function of amplitude interval [0,1], see Table 1. This corresponds to starting the evolution with low energy jamming techniques and mutating more energy rich solutions, producing lower detectability, along the way, forming a rough and approximate Pareto front over the evolutionary time. However, this 'growing' method does not ensure that the best Pareto front is found, and multi-objective evolutionary algorithms (MOEA) methods are often used for finding the optimal Pareto front. Using the NSGA-II [1] MOEA we are able to compare MOEA final population to single-objective GA (SOGA) evolution. In Table 2 NSGA-II GA Toolbox settings are presented.

In Figure 7a NSGA-II results are compared to SOGA results for different creation intervals and different fitness functions. Figure 7a shows that no method comprises the Pareto front alone. The NSGA-II optimization method forms the Pareto front on the central region of the problem domain, but has problems reaching the extremes on both axes. 25631 generations were used to produce NSGA-II result, equivalent to 5.62 CRC.

Table 2: MATLAB GA Toolbox parameters for NSGA-II

Creation:	Uniform	Interval [0,100]	Population Size 15×121
Selection:	Binary Tournament	Rank Fitness Scaling	Elitism included
Crossover:	Scattered	Crossover Fraction 0.8	
Mutation:	Gaussian	Scale 0.01	Shrink 0

The SOGA using the 'growing' method forms the Pareto front for *J/S* above ~10. Furthermore, using the 'growing' method and including *J/S* in the SOGA fitness function, results comparable to the NSGA-II part of the Pareto front can be achieved. Using different creation function amplitude intervals do not improve SOGA results when compared to the 'growing' method. Lines marked with 'C' in Figure 7a have been created on the same initial amplitude interval as the NSGA-II optimizations.

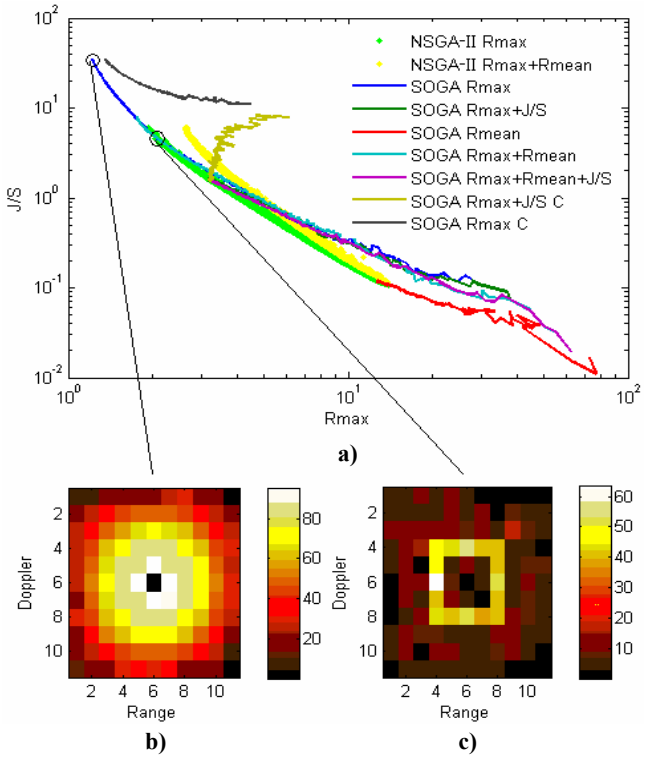

Figure 7: The Pareto front. a) shows the combined Pareto front for single- and multi-objective optimization methods using different creation functions and fitness functions. Two jamming techniques on the Pareto front having b) *J/S*=34.471 and R_{max}=1.221 after 129118 generations and c) *J/S*=4.001 and R_{max}=2.197 after 500 generations.

Finally, the SOGA fitness function of R_{mean} produces the Pareto front for the not so interesting region of *J/S* below 0.01 and R_{max} above 10. This fitness function is not capable of producing results extending from this region, making it unsuitable for further studies. Using R_{max}+R_{mean} as fitness function does not significantly improve performance compared to R_{max} for neither SOGA nor NSGA-II methods.

Figure 7b and 7c show two different jamming techniques on the Pareto front. Jamming technique 7c exhibits the same jamming structure as the jamming matrix of Figure 5. However, the new jamming technique is Pareto preferred having a combined lower *J/S*~4, lower R_{max}~2.2 and lower CRC~0.0061. In Figure 7b a jamming matrix with a performance of *J/S*~35 and R_{max}~1.2 is produced after 1.56 CRC. This new type of jamming technique is the result of raising the surroundings of the low *J/S* jamming matrix structure over the course of evolutionary time into a 'Gaussian' like jamming signal structure.

4.2 Noise Analysis

Jamming technique optimization has been done on the radar RD matrix without noise. When including noise in the system the radar RD CFAR ratio matrix will be dominated by noise detections making it difficult to find jamming codes with high *J/S* and low detectability. Moreover, at least in the initial phase of the study the system should be as simple as possible in order to facilitate relevant jamming technique findings. However, any effective jamming

technique used in a real environment must be noise-robust and able to handle thermal noise. Hence, the effect of including thermal noise in the system, as given by Equation 1, is analysed. Using a CFAR frame of 5×5 and evaluating noise only distributions, the resulting radar RD CFAR ratio matrix statistics can be described by

$$R_{CFAR5\times5,mean}\left(N\left(0,\sigma\right)\right)=1.04\pm0.83 \qquad (2)$$

This shows that the CFAR ratios are independent of thermal noise levels in the radar RD matrix.

The detectability measure R_{max} evaluated without noise in the system results in an abrupt transition of a CFAR threshold producing no detections above R_{max} and certain detections below R_{max}. Introducing noise in the system will widen this transition phase for the CFAR threshold, as illustrated in Figure 8a, where the jamming technique of Figure 7c produces R_{max}=2.1972 when evaluated without noise. Figure 8b shows the radar RD CFAR ratio matrix including a noise distribution given by $N(0,5)$. In Figure 8c the resulting radar RD CFAR ratio statistics of 1000 different noise distributions for the target pixel are histogrammed, showing a blurring of the detection probability region for the CFAR ratio threshold where P_{det}=0.5 is given by R_{mean}=2.1974±0.251.

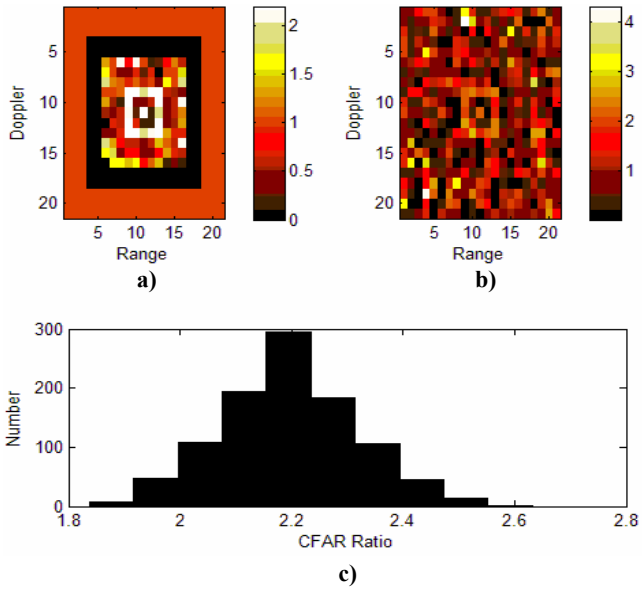

Figure 8: Example of including thermal noise. a) is radar RD CFAR ratio matrix of jamming matrix in Figure 7c without noise. b) is the corresponding radar RD CFAR ratio matrix with noise given by $N(0,5)$. c) is the histogram of 1000 noise evaluations producing R_{mean}=2.1974±0.251 for the target pixel.

In Figure 9 the mean CFAR ratio and standard deviation for the jamming techniques of Figure 7 are evaluated for different noise statistics. This figure shows that the mean CFAR ratio when including noise in the system is lower than the maximum CFAR ratio evaluated without noise. This proves that the jamming techniques are noise-robust even though we optimized without noise.

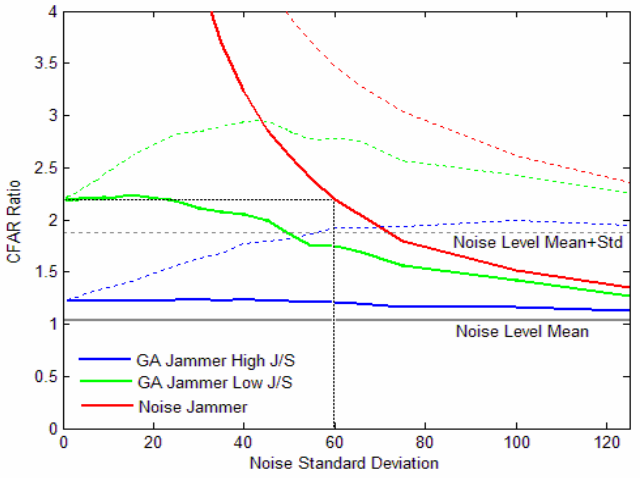

Figure 9: Noise analysis for the techniques of Figure 7 showing mean CFAR ratio (solid) and including standard deviation (dotted) for the radar RD CFAR ratio matrix target pixel. The GA techniques are compared to a noise jammer.

Furthermore, Figure 9 shows the increasing CFAR ratio standard deviation when noise is included in the system, widening the transition phase between certain detection and no detection for the CFAR threshold. As noise levels increase, the CFAR ratio standard deviation reaches the same magnitude as the noise only CFAR ratio standard deviation, making the CFAR ratio matrix noise dominant.

Comparing GA jamming techniques to more conventional jamming techniques result in a measure on GA technique performance. A conventional noise jammer [5] emits white noise as given by Equation 1 filling the entire RD matrix of the radar. In Figure 9 the GA jammer techniques are compared to a conventional noise jammer on a 21×21 radar RD matrix, finding that $R_{mean,noise\text{-}jammer}=R_{max,GA\text{-}jammer}$ at $N(0,60)$ equal to $J_{noise\text{-}jammer}/S$~160, which is 40 times more transmitting power than the GA technique. This number would increase to ~1100 if the noise jammer was to be evaluated on a 95×127 matrix.

4.3 Dynamic Target RCS Optimization

Target RCS is highly sensitive to target orientation relative to the radar [12]. In a real world situation the jammer would probably not be able to have an accurate estimate of the true target RCS at all times. The RCS of the target is now 10 samples from a normally distributed cross section given by

$$RCS_{dynamic}=N\left(\mu=RCS_{static},\sigma=\mu/2\right) \qquad (3)$$

where $\mu=RCS_{static}$=100 and using mean R_{max} from all the 10 RCS samples as the fitness function. Pseudo code of dynamic target RCS optimizations is given next.

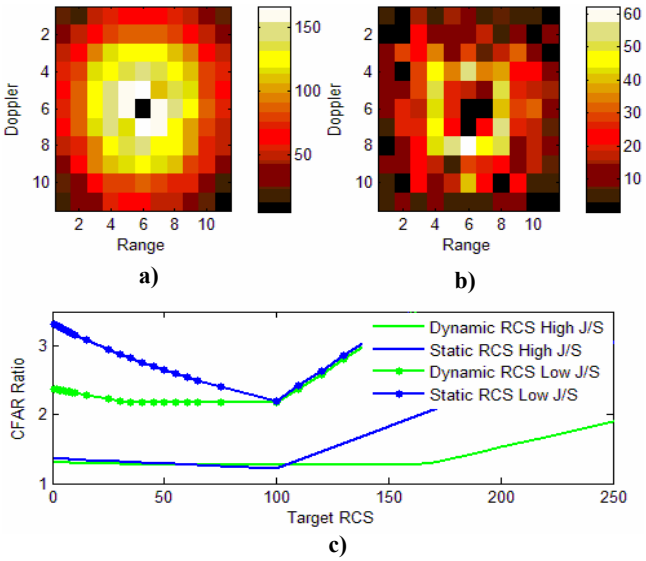

Figure 10: Varying target RCS analysis. a) is jamming matrix optimized using dynamic RCS for high *J/S*=103.4091 and R_{max}=1.2262 after 7188 generations and b) is low *J/S*=6.332 and R_{max}=2.182 after 682 generations, both for *RCS*=100. In c) the techniques are analysed for varying RCS and compared to the techniques of static RCS in Figure 7.

```
for i=1:populationSize %loop over population
 for j=1:numberOfRCSevaluations %set to 10 samples
  GetJammerRDMatrix(GetChromosome(population,i))
  TargetRDMatrix(tgtRange,tgtDoppler)=RCS(N(μ,σ))
  GetRadarRDMatrix(JammerRDMatrix,TargetRDMatrix)
  GetRadarCFARRatioMaxtrix(RadarRDMatrix,CFARtype)
  R(j)=max(RadarCFARRatioMaxtrix)%get Rmax for RCS
 end
 F=mean(R) %report mean fitness for RCS
end
```

Results of the dynamic target RCS optimization of jamming techniques for high *J/S* and low *J/S* are shown in Figure 10a and 10b, requiring 0.87 and 0.083 CRC respectively. In Figure 10c the detection performance for the two techniques is plotted for different target RCS and compared to the static RCS optimization techniques of Figure 7. The low *J/S* jamming technique from dynamic target optimization shows much improved detection performance for target RCS below 100 when compared to the static case of same detectabilty. The dynamic technique exhibits almost flat detection performance in this region at an increased cost of ~1.5 times the static jamming technique *J/S*. For the high *J/S* jamming techniques, the two cases are quite similar below 100, but the dynamic technique extends its good performance into a RCS of almost 170 producing *J/S*~35 at that RCS. This is comparable to the static jamming technique of high *J/S*. Overall, this shows that dynamic target RCS optimization improves robustness against variations in target RCS for low *J/S* techniques more than for high *J/S* jamming techniques.

5. MULTI-RESISTANT JAMMING

In this section the second objective in the jammer objective list in section 3 is addressed, allowing for the possibility of an unknown radar CFAR detection algorithm. In Figure 11 three different but general CFAR frames are shown, representing the different possible CFAR algorithms we want to optimize against. As a result, we study the possibility of developing one single jamming code which is able to counter all three CFAR algorithms simultaneously, making the jamming technique multi-resistant. Pseudo code of such multi-resistant optimization is shown below.

```
for i=1:populationSize %loop over population
 GetJammerRDMatrix(GetChromosome(population,i))
 GetRadarRDMatrix(JammerRDMatrix,TargetRDMatrix)
 GetRadarCFARRatioMaxtrix(RadarRDMatrix,CFARtype1)
 GetRadarCFARRatioMaxtrix(RadarRDMatrix,CFARtype2)
 GetRadarCFARRatioMaxtrix(RadarRDMatrix,CFARtype3)
 Rmax1=max(Radar1CFARRatioMaxtrix)%get Rmax1
 Rmax2=max(Radar2CFARRatioMaxtrix)%get Rmax2
 Rmax3=max(Radar3CFARRatioMaxtrix)%get Rmax3
 F=Rmax1+Rmax2+Rmax3 %report the combined fitness
end
```

Target signature is static 100 and the fitness function used is the linearly combined R_{max} of the three different CFAR types.

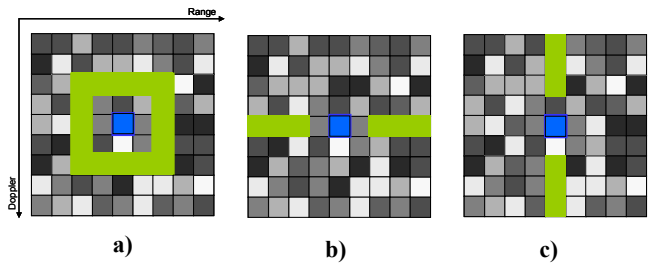

Figure 11: Three CFAR frames of a) 5×5, b) 3×1 and c) 1×3, representing different types of CFAR algorithms.

5.1 The Pareto Front

In Figure 12a the Pareto front for the multi-resistant jamming technique is shown. Pre-analysis showed insignificant differences in performance for the 13×13 and 15×15 jamming matrices, leaving the 11×11 jammer matrix as the preferred matrix size for multi-resistant technique development. Using both SOGA and NSGA-II optimization methods, see Table 1 and Table 2 for parameter settings, the single-resistant jamming technique against the 5×5 CFAR frame is found to perform slightly better than that of the multi-resistant case. This is not surprising since the multi-resistant jamming technique also has to accommodate the 3×1 and 1×3 CFAR frames. Nevertheless, the high *J/S* multi-resistant jamming technique of Figure 12b converges on the high *J/S* single-resistant Pareto front for the 5×5 case. The Pareto front for the CFAR frame of 3×1 in Figure 12a exhibits similar performance as that of the 5×5 frame, demonstrating multi-resistant properties for the jamming techniques developed. The 1×3 case is not shown due to symmetry considerations. In Figure 12c a low *J/S* multi-resistant jamming technique, which is comparable to the single-resistant jammer matrix of Figure 7c, is shown. The 'structure' of this new technique shows how the energy is deposited on the combined CFAR frames in a complex manner and the slight raising of the surrounding energy floor. Energy expenditure of this new technique increases by a factor of approximately 1.5 compared to the single-resistant case and raises the need for computing time to 3.44 and 0.032 CRC for high and low *J/S* techniques. NSGA-II results used 1.78 CRC.

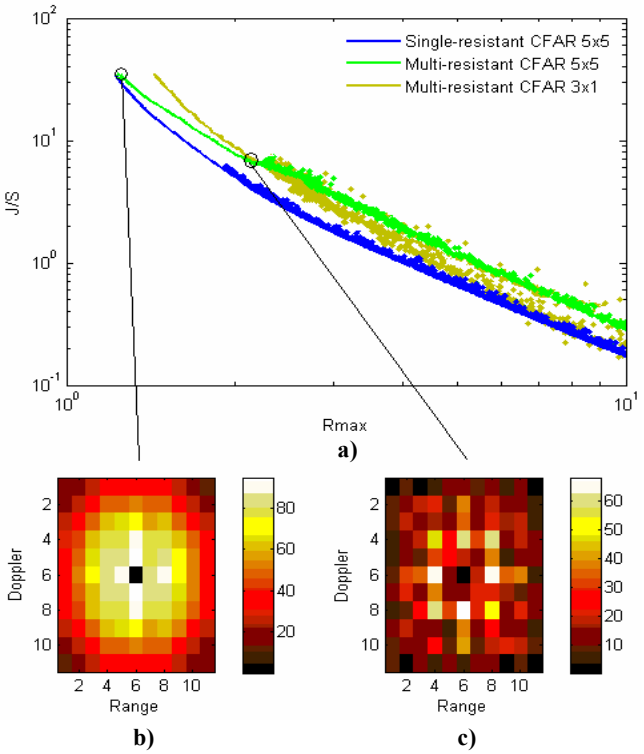

Figure 12: In a) the Pareto front for the multi-resistant technique optimization is compared to the single-resistant case of CFAR frame of 5×5. b) is the jamming matrix of *J/S*=35.36 with $R_{max,5\times5}$=1.2373 and $R_{max,3\times1}$=1.4325 after 94862 generations. c) is the technique of *J/S*=6.459 with $R_{max,5\times5}$=2.1976 and $R_{max,3\times1}$=2.2649 after 891 generations.

5.2 Noise Analysis

In Figure 13 and 14 the jamming techniques of Figure 12b and 12c are evaluated for different thermal noise statistics. In Figure 13 the high *J/S* multi-resistant jamming technique is compared to the single-resistant jamming technique of Figure 7b for the 5×5 case.

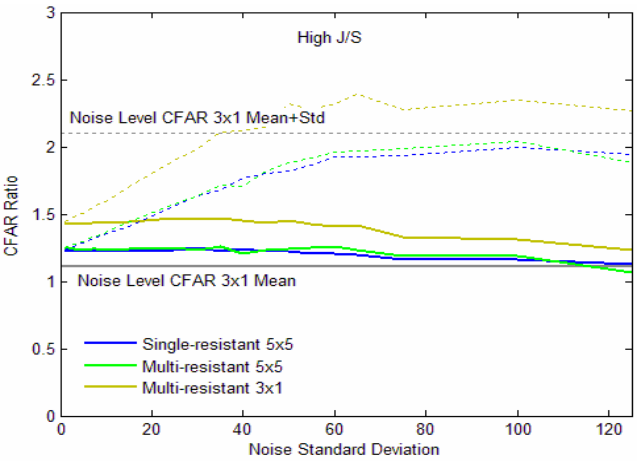

Figure 13: Noise analysis for high *J/S* techniques of Figure 7b and Figure 12b is compared. Mean CFAR ratio is solid lines and including standard deviation is dotted lines.

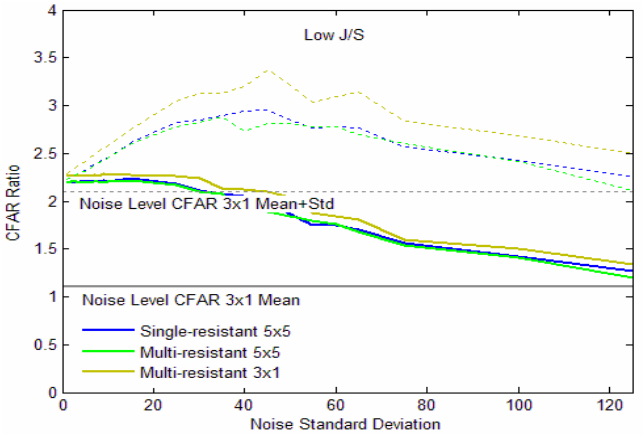

Figure 14: Noise analysis for low *J/S* techniques of Figure 7c and Figure 12c is compared. Mean CFAR ratio is solid lines and including standard deviation is dotted lines.

This comparison shows no significant changes in noise robustness. The 3×1 case shows good noise robustness when compared to the noise statistics of $R_{CFAR3\times1,mean}$= $R_{CFAR1\times3,mean}$ =1.11±0.99, which is slightly higher than the 5×5 statistics from Equation 2. In Figure 14 the low *J/S* multi-resistant jamming technique is compared to the single-resistant technique from Figure 7c, exhibiting similar good noise robustness as the high *J/S* technique.

5.3 Dynamic Target RCS Optimization

Allowing for dynamic target RCS using Equation 3 and the mean R_{max} of 10 RCS samples, robustness against target RCS variations for the multi-resistant jamming techniques is investigated.

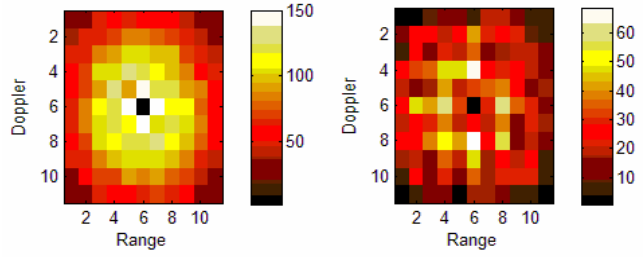

Figure 15: Varying target RCS optimization for multi-resistant techniques of a) high *J/S*=85.4435 with $R_{max,5\times5}$=1.4163 and $R_{max,3\times1}$=1.4812 after 6562 generations and b) low *J/S*=8.6663 with $R_{max,5\times5}$=2.1978 and $R_{max,3\times1}$=2.1557, after 999 generations, both at RCS=100.

In Figure 15 the high and low *J/S* jamming techniques from dynamic target RCS optimizations are shown, requiring 2.38 and 0.363 CRC respectively. In Figure 16a both techniques are compared to the static multi-resistant jamming techniques found previously for the 5×5 CFAR frame cases. As shown in section 4.3, the low *J/S* multi-resistant techniques benefit more from dynamic target RCS optimization than the high *J/S* jamming matrices. In Figure 16b the same matrices are compared for the 3×1 CFAR frame case, showing that the low *J/S* jamming techniques have a higher increase in performance than the high *J/S* jamming techniques as well.

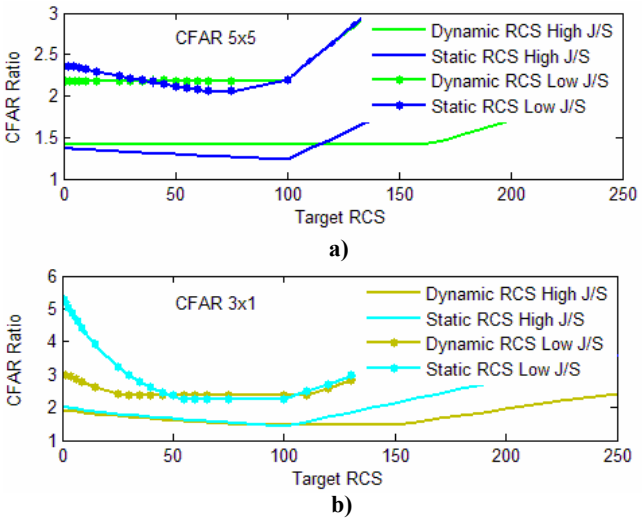

Figure 16: Varying target RCS analysis for multi-resistant techniques of Figure 15a and b. a) and b) show the mean CFAR ratios for different target RCS for 5x5 **and** 3x1 **CFAR frames respectively. Static techniques are from Figure 12.**

6. SUMMARY AND CONCLUSION

In this paper the applicability of using GA for developing efficient jamming techniques for advanced DRFM jammers against radars employing CFAR detection algorithms has been successfully demonstrated. Using GA, new types of jamming techniques have been developed and fresh insight into the complex radar-jammer dynamics is gained, proving that GA is a highly efficient optimization method capable of handling the large and complex solution space of our problem. Furthermore, at the expense of a small increase in jamming transmitting power, effective multi-resistant GA jamming techniques have been developed. In real life operations, when confronted with uncertain type of radar CFAR detection algorithms, multi-resistant jamming techniques are of high importance. This ability to produce multi-resistant GA jamming techniques demonstrates the unique potential and exceptional strength of evolutionary algorithms for optimizing advanced DRFM jammers for future radar jamming applications.

Even though optimization is done without noise in the radar-jammer system the jamming techniques developed are shown to be effective in noisy environments. This proves that GA jamming techniques, both single- and multi-resistant, are noise robust. Comparing GA jamming to more conventional noise jamming, advanced DRFM jammers are found to produce highly energy efficient jamming techniques.

In real scenarios a jammer is probably not able to assess the true target RCS at all times. Although increasing *J/S* about 1.5 times, dynamic target RCS optimization of jamming codes is found to compensate for this target property. Whereas high *J/S* techniques seem to have some intrinsic robustness against dynamic target RCS, the low *J/S* jamming techniques benefit more from such dynamic optimization.

The ability to find a Pareto front in the problem domain of jammer transmitting power versus detectability is an important one as seen from an ECM decision-maker's point of view. Having found a Pareto front one can easily apply standard operational analysis methods for finding the appropriate jammer settings for a particular scenario. For the time being, we are satisfied with a well performing Pareto front, finding two new types of jamming techniques of high and low *J/S* within the reasonable CPU expenditure of 6.1×10^6 to 5.69×10^9 CFAR ratio calculations. However, finding the optimal Pareto front using one single efficient method could be a challenge. In order to explore this issue further, experimentation with NSGA-II settings or implementing other multi-objective evolutionary algorithms, possibly including hybrid schemes, is needed.

Finally, the third objective in the jammer objective list, included for completeness, is not addressed in this paper. This is due to the fact that radar and jammer parameter variations and their interactions are a highly complicated matter. Instead of complex and detailed simulations this suggests experimenting with real radars and jammers, an analysis pending a soon available lab based radar asset.

7. REFERENCES

[1] Deb, K., Pratap, A., Agarwal, S. and Meyarivan, T., "A Fast and Elitist Multiobjective Genetic Algorithm: NSGA-II", *IEEE Transactions on Evolutionary Computation*, vol. 6, no. 2, pp. 182-197, April 2002.

[2] Goldberg, D. E. *Genetic Algorithms in Search, Optimization and Machine Learning*. Addison-Wesley Longman Inc., 1989.

[3] Hong, S. et al., "Investigation on Genetic Algorithm for Countermeasures Technique Generator", *Proceedings on ISSSE'07*, pp. 351-354, 2007.

[4] Høydal, T.-O., "Advanced Digital Radio Frequency Memory (DRFM) Technology – New Capabilities for Intelligent Radar Electronic Countermeasures", *ATEDS/SA Symposium and Exibition*, San Diego, USA, March 2001.

[5] Lothes, R. N., Szymanski, M. B. and Wiley, R. G. *Radar Vulnerability to Jamming*. Artech House, Inc., 1990.

[6] Nunez, A. S. et al., "ECM Techniques Generator", *Modeling and Simulation for Military Applications - Proceedings of the SPIE*, vol. 6228, pp. 62280Z, 2006.

[7] Kristoffersen, S. and Thingsrud, Ø.,"The EKKO II Synthetic Target Generator for Imaging Radar", *Proceedings of EUSAR 2004*, vol 2, pp. 871-874, May 2004.

[8] MATLAB Genetic Algorithm and Direct Search Toolbox™ 2.2, ©1994-2008 The MathWorks, Inc.

[9] McGrath, M., "ECM Techniques Generator", *Proceedings of 48th Midwest Symposium on Circuits and Systems*, vol. 2, pp. 1749-1752, 2005.

[10] Pace, P. E., Fouts, D. J., Ekestorm, S. and Karow C., "Digital False-Target Image Synthesiser for Countering ISAR", *IEE Proceedings - Radar, Sonar and Navigation,* vol. 149, no. 5, pp. 248-257, October 2002.

[11] Schleher, D. C. *Electronic Warfare in the Information Age.* Artech House, Inc., 1999.

[12] Skolnik, M. *Radar Handbook*, 2nd edition, McGraw-Hill, Inc., 1999.